Foliar Delivery of siRNA Particles for Treating Viral Infections in Agricultural Grapevines

Aviram Avital[1,2,†], Noy Sadot Muzika[3,†], Zohar Persky[3,†], Gili Bar[1], Yuval Michaeli[1], Yulia Fridman[4], Avishai Karny[1], Jeny Shklover[1], Janna Shainsky[1], Sigal Savaldi-Goldstein[4], Haim Weissman[5,], Oded Shoseyov,[3,*] Avi Schroeder[1,*]*

[1]Laboratory for Targeted Drug Delivery and Personalized Medicine Technologies, Department of Chemical Engineering, Technion – Israel Institute of Technology, Haifa 3200003, Israel
[2]The Norman Seiden Multidisciplinary Program for Nanoscience and Nanotechnology, Technion – Israel Institute of Technology, Haifa 3200003, Israel
[3]Robert H. Smith Faculty of Agriculture, Food and Environment, Hebrew University, Rehovot 76100, Israel
[4]Faculty of Biology, Technion - Israel Institute of Technology, Haifa 3200003, Israel
[5]The Weizmann Institute of Science, Department of Organic Chemistry, Rehovot 76100, Israel
† Equal contribution

*To whom correspondence should be addressed:
Prof. A.S. avids@technion.ac.il
Prof. O.S. shoseyov@agri.huji.ac.il
Dr. H.W. haim.weissman@weizmann.ac.il

Keywords: viral disease, nanotechnology, siRNA, RNAi, agriculture.

Abstract

Grapevine leafroll disease (GLD) is a globally spreading viral infection that causes major economic losses by reducing crop yield, plant longevity and berry quality, with no effective treatment. Grapevine leafroll associated virus-3 (GLRaV-3) is the most severe and prevalent GLD strain affecting wine production. Here, we evaluated the ability of RNA interference (RNAi), a non-GMO gene-silencing pathway, to treat GLRaV-3 in infected Cabernet Sauvignon grapevines.

We synthesized lipid-modified polyethylenimine (lmPEI) as a carrier for long double-stranded RNA (dsRNA, 250-bp-long) that targets RNA polymerase and coat protein genes that are conserved in the

GLRaV-3 genome. Self-assembled dsRNA-lmPEI particles, 220 nm in diameter, displayed inner ordered domains spaced 7.3±2 nm from one another, correlating to lmPEI wrapping spirally around the dsRNA. The particles effectively protected RNA from degradation by ribonucleases and showed to increase uptake rate into plant cells as a result of the lipid component comprising the RNA carrier. In three field experiments, a single dose of foliar sprayed treatment of the RNA-particles knocked down GLRaV-3 titer, and multiple doses of the treatment kept the viral titer at baseline and triggered recovery of the vine and berries.

This study demonstrates RNAi as a promising platform for treating viral diseases in agriculture.

1. Introduction

The wine industry in both ancient and modern times depends greatly on healthy vines and fine grapes.[1] In recent decades, viral grapevine leafroll disease (GLD) poses a major economic threat to wine production by reducing crop yield and hampering grape quality including cluster size, pH, sugar level and color.[2] Among eleven viruses associated with GLD, grapevine leafroll associated virus 3 (GLRaV-3) is the most prevalent and severe strain inducing robust symptoms by decreasing plant vigor and longevity.[3] In New Zealand, for example, GLRaV-3 delayed the ripening of Sauvignon Blanc berries and reduced their acidity.[4] In Benton Harbor, Michigan, yield per vine along with soluble solids content declined in infected Cabernet Franc vines.[5]

Genetically, GLRaV-3 belongs to the *Ampelovirus* genus and consists of helical, positive sense single stranded RNA (ssRNA) genome approximately 18.5 kb in size.[6] The virus has 12 open reading frames coding for replication and structure-related proteins such as RNA dependent RNA polymerase (RdRp) and coat protein (CP), respectively, among other essential proteins.[7] Current approaches for dealing

with GLD include uprooting and incinerating infected vines to curb virus transmission and progression.[8] Thus, new technological approaches are warranted in order to mitigate GLD's negative impact.

RNA interference (RNAi) is a gene regulation mechanism also known as post-transcriptional gene silencing (PTGS).[9] This mechanism is sequence-specific due to its dependency on double stranded RNA (dsRNA) precursors to trigger gene silencing,[10] although ssRNA precursors were shown to share the same RNAi pathway but result in lower efficiency.[11] In plants, RNase III-like enzyme, dicer-like protein, processes dsRNA into 21-24 bp short interfering RNA (siRNA) which guide transcript recognition and degradation downstream.[12] Unlike mammalian cells, dicer-like protein preferably processes long dsRNA sequences to yield multiple siRNAs which transfer between plant cells via plasmodesmata.[13] In order to utilize RNAi, dsRNA needs to enter the cell cytoplasm. RNA particles, complexed with lipids and polymers, have been used for triggering RNAi in medicine and aquaculture.[14] Direct foliar application of naked dsRNA may result in RNA degradation prior to penetrating the cell. In addition, standard delivery methods (e.g., *Agrobacterium* and DNA vectors) have limitations of their own such as off-target effects, while formulation can extend the silencing duration and specificity.[15]

Here, we evaluate a delivery platform for long dsRNA based on lipid-modified polyethylenimine (lmPEI) for efficient systemic silencing of GLRaV-3 in grapevines. We assessed the ability to use RNAi for treating viral infections in grapevines. dsRNA-lmPEI particles synthesis is rapid and scalable resulting in stable particles in ambient conditions. We chose to apply the RNA particles via canopy spraying, which is the common and practical route of administration among wine growers.[16] In addition, dsRNA-lmPEI particles are shown to protect the RNA payload from ribonuclease activity and

trigger GLRaV-3 viral knockdown in three consecutive field experiments following foliar administration. Altogether, this study opens a frontier for using RNAi to treat viral infections in grapevines.

2. Results and Discussion

2.1. Preparation and characterization of dsRNA-lmPEI particles

We synthesized lmPEI as a RNA carrier and tested its effect on GLRaV-3 titer in grapevines. Briefly, 14-carbon lipid was conjugated to branched PEI in a 3:1 (epoxide tail:PEI head group) molar ratio to form lmPEI. The product was purified using multiple phase separation steps, and ^{1}HNMR spectra revealed a peak at 3.62 ppm corresponding to a hydroxyl functional group that confirms the successful conjugation of lipids tails to the PEI (Figure S1). Next, 250 bp dsRNA was complexed with lmPEI under acidic conditions (pH=5.2) to establish electrostatic interactions between the negatively charged dsRNA and cationic lmPEI, to formulate dsRNA-lmPEI particles, as illustrated in Figure 1A. To target GLRaV-3's ability to replicate and assemble, we chose to knockdown RNA-dependent RNA polymerase and coat protein genes using two conserved sequences (Figure S2A and S2B). The sequence design excluded unintended off-targets within the GLRaV-3 and wine grapevine (e.g., *Vitis vinifera*) genomes. The dsRNA length was optimized to trigger the dicer-like protein at different locations along the sequence to generate multiple siRNAs and increase knockdown probability (Figure S2C).[14, 17]

To be effective, the dsRNA-lmPEI particle must bind, protect, and release the RNA at the target site.[18] Since binding and release rely on lmPEI electrostatic affinity to dsRNA, they can be controlled through the N:P ratio. In our study, the N:P ratio is defined as the molar ratio between positively charged amine groups present in lmPEI and negatively charged phosphate groups present on the dsRNA

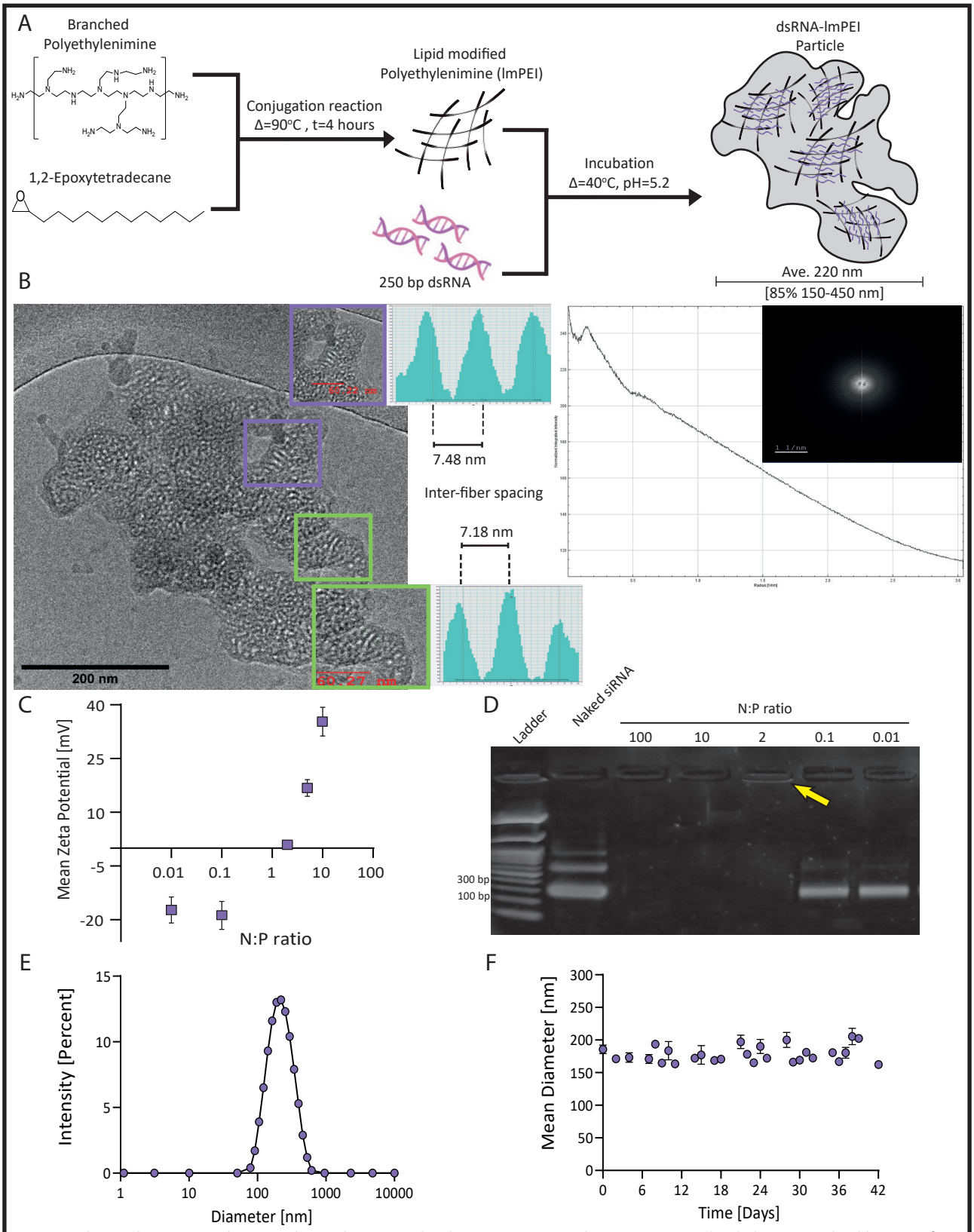

Figure 1: dsRNA-lmPEI particles Particle synthesis: Lipid tails were conjugated to a cationic polyethyleneimine backbone to form lipid-modified polyethylenimine (lmPEI). lmPEI was complexed with negatively charged dsRNA into sub-micron particles. These particles had a surprising inner-ordered structure (A). cryoTEM image presenting dsRNA-lmPEI particle with inner ordered domains and its fast fourier transformation (FFT) histogram (B). Enhanced insets show gray values profile measurements indicating inter-fiber spacing (7.3±2 nm) from one dsRNA center of mass to another, suggesting a structure correlating to lmPEI wrapping spirally around the dsRNA. We examined particles with different PEI-amine:RNA-phosphate (N:P) ratios according to their Zeta potential (N=3, C) and capacity to complex with 250-basepair-long dsRNA, analyzed by gel electrophoresis (2% agarose, 100V, 35 minutes, D). At low N:P ratios (0.01 and 0.1), bands signify unbound dsRNA matching to naked dsRNA. The yellow arrow highlights band corresponding to complexed dsRNA (0.91±0.08 mV) indicating successful complexation. Particles were tested for their size distribution using dynamic light scattering, peaking at 220 ± 7.75 nm (E). Particles' stability was coherent for over 40 days at room temperature, 25mM sodium acetate, pH=5.2, with no significant change in size measured (F).

backbone. To determine this ratio, a constant weight of dsRNA was converted to its equivalent phosphate mole and lmPEI was conjugated accordingly to reach the desired mole of protonated amines. Increasing the N:P ratio elevated the particle's surface charge (Figure 1C), while below an N:P ratio of 2 (i.e., 0.01 and 0.1) particles were not formed, indicating insufficient lmPEI to bind dsRNA (Figure 1D). Therefore, we conducted our next experiments using N:P=2 particles which bind dsRNA, carrying a weak positive charge (0.91 ± 0.08 mV). The encapsulation efficiency of dsRNA was 92% (Figure S3) and the particle size averaged 220 nm (Figure 1E) with 85% of particles ranging 150-450 nm. The dsRNA-lmPEI particles were imaged using cryo-TEM. Low and high contrast patterns indicate fibrillar high contrast aggregated structure. Some domains exhibited local order within the particle. The high contrast features correspond to sp^2 carbons of the π-stacked system representing dsRNA and the low contrast represents sp^3 hybridized atoms of the lmPEI, respectively.[19] Relevant radial integration of fast fourier transform (FFT) of the imaged particle was employed in the investigation of the inner structure of the particles (Figure 1B). Previous studies have shown that DNA/PEI complexation is highly kinetic. This is due to electrostatic forces, the main driving force for binding, being affected by the percentage of protonated groups within PEI.[20] Inter-fiber spacing between one dsRNA center of mass to another was 7.3 ± 2 nm, as observed from the FFT and from the gray values profile measurements (see insets in Figure 1B; additional measurements are found in Figure S4). This spacing seems to be due to the lipid tails presence within the particle and their protrusion out from the polymeric backbone enabling possible interaction with other lmPEI molecules attached to other parts of the dsRNA fiber. The lipophilic character of the alkylic chains of the lmPEI also contribute to the aggregate formation in the aquatic environment as observed in the cryo-TEM image and from partially energy minimized molecular mechanics model (Figure S5). Similar to the proposed model by

Ziebarth and colleagues,[21] our findings may also show a possible model of lmPEI wrapping around dsRNA in a spiral manner. Finally, we tested the particle size as a measure of stability and did not notice significant changes over a period of 40 days (Figure 1F).

2.2. Particle penetration and biodistribution in the leaf and vine

We evaluated the ability of dsRNA-lmPEI particles to penetrate and distribute within vines. The lmPEI carrier was covalently labeled with a Cyanine 5 (Cy5) and then complexed with dsRNA. Treatment groups (N=5 per group) received five different treatments: free Cy5 or Cy5 labeled particles, each given by spray and immersion methods, and 25 mM sodium acetate buffer (control). The immersed leaves' petioles were embedded within 600 µl of treatment solution while sprayed leaves were treated with 10 mL of relevant infiltrate to cover both their ventral and dorsal sides. The accumulation of particles was imaged and quantified 2 hours after the treatment, and six different locations were used to record the full plant biodistribution profile. Basal autofluorescence was recorded at the initial time and accumulation was seen in both spray and immersion administrations after the 2-hour treatment (Figure 2A, control is presented in Figure S6). Particle accumulation was visualized within both the primary and secondary veins of a leaf when its petiole was immersed within labeled particles, in contrast to sprayed treatment where fluorescence was dispersed throughout the leaf and no particle accumulation was seen within the veins. Moreover, the signal in the immersed leaves after 2 hours significantly increased as demonstrated by quantification of both the average intensity and the number of particles ($P<0.05$ and $P<0.001$, respectively Figure S7). These results suggest particles can penetrate through the stomata after spraying as well as enter a leaf's veins following immersion, ultimately distributing within the vine.

To quantify the biodistribution of the particles in the plant tissue lmPEI particles were covalently conjugated to Gadolinium ($GdCl_3$) using a DOTA chelator group. Then, Gd-labeled particles were administered to vine leaves by submersion for 72 hours. Gd concentration was quantified in the plant tissues (leaves, petioles, stem, and roots) located up to 25 cm above or below the application point, using elemental analysis (Figure 2C). Interestingly, Gd concentrations were similar above and below the application point, suggesting that the particles enter the leaf and translocate in the plant through the phloem vascular pathway. The phloem, a tissue mainly responsible for trafficking photosynthesis products from the leaves to the rest of the plant, is a primary harboring tissue of the GLRaV-3 virus in the vine.[3] Overall, both qualitative microscopy and quantitative elemental analysis suggest that lmPEI-dsRNA particles distribute systemically within the vine.

We further examined the effect of the lipid component on particle uptake into transgenic *Arabidopsis* roots expressing a plasma membrane-localized fusion protein GFP–LTI6b to mark the cell surface. Lipidated and non-lipidated PEI was complexed with RNA to form nanoparticles, which were then administered hydroponically to the roots before live imaging. The uptake of the particles was traced by covalently labeling the Cy5 dye to the PEI backbone, and then using confocal microscopy to image the roots over time. Treatment groups (N=4 per group) included five different treatments: 1) Cy5-labeled lipidated and 2) non-lipidated particles; 3) non-labeled lipidated and 4) non-lipidated particles and 5) free Cy5 (control). Roots were placed on an optical plate under a semi-permeable medium followed by an administration of a 20 µl treatment solution. Particles' accumulation was imaged and quantified at initial time and after 3 hours (Figure 2D, left and right panels, respectively). Accumulation dynamics showed that particles penetrated better through the elongation region rather than to meristematic zone thus creating a signal gradient from epidermis inwards. This observation

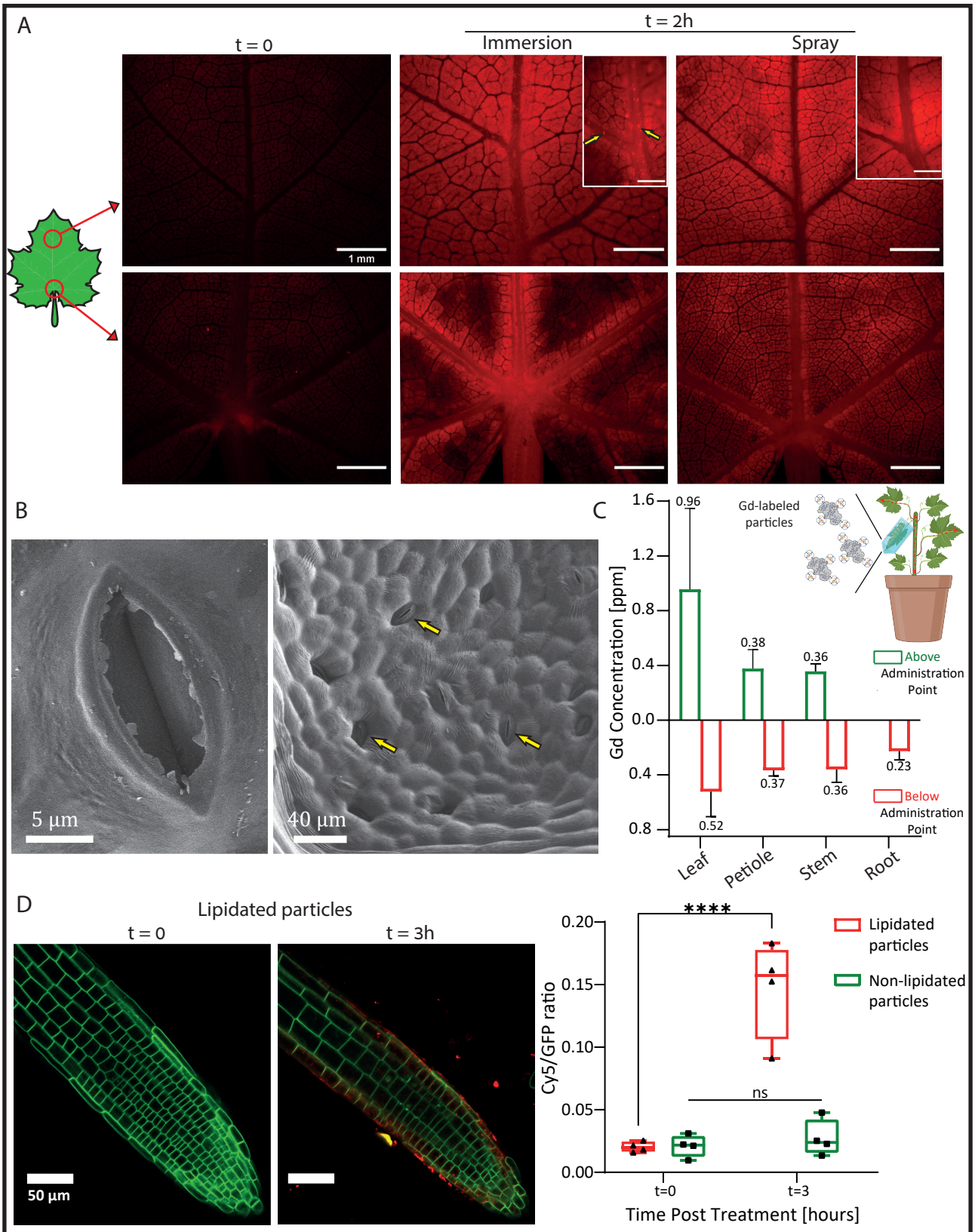

Figure 2: Particle penetration and biodistribution Distribution of Cy5-labeled particles within vine leaves after a 2-hour administration via spray or immersion (scale bar - 1 mm, A). Particle accumulation is observed within leaf veins after 2 hours, marked with yellow arrows in the upper middle inset (scale bar - 500 µm). Vine leaf's HR-SEM image shows multiple stomata on the leaf surface (B, right panel, emphasized by yellow arrows). Open stomate dimension measured 6.105 µm wide and a 16.14 µm long, being a possible route for dsRNA-lmPEI particle penetration into the plant (B, left panel). Vine seedlings' leaf was submerged in an aqueous solution of Gd-conjugated particles, for 72 hours. Gadolinium concentration was quantified in plant tissues above (green) or below (red) the administration point (C). Uptake and accumulation of lipidated particles was recorded 3 hours after administration to roots of transgenic Arabidopsis expressing plasma membrane localized GFP (D, left panel). Particle uptake increased by 7.35-fold for lipidated particles in comparison to particles that lack lipid tail, indicating the effect of the lipid presence in formulation facilitates uptake into plant cells (N=4, D, right panel). Results are shown as mean ± SD. Ordinary two-way ANOVA test was used for the statistical analysis of D. ns – not significant, ****p<0.0001.

may be attributed to low permeability of lateral root cap cells covering root tip (meristem).[22] Particle uptake was quantified by measuring the Cy5 normalized to the plants' GFP signal over time. Lipidated particles showed a significant 7.35-fold increase in uptake ($P<0.0001$, Figure 2D, right panel) compared to non-lipidated particles, that kept the same uptake ratio over 3 hours (Figure S8). This indicates that the lipid component in the RNA carrier plays a significant role in interacting with root epidermal tissue uptake.

To gain further knowledge regarding particle penetration pathways into the plant, lower (abaxial) and upper (adaxial) sides of an infected leaf were imaged via high resolution scanning electron microscopy (HR-SEM). Stomata are seen scattered throughout abaxial surface epidermal tissue (Figure 2B). Size measurements of the stomate showed a 6.105 μm width and a 16.14 μm length opening, which can facilitate a port of entry for the nanoparticles. Apart from stomatal penetration, previous studies showed evidence of polar solute diffusion path across plant cuticle via "polar pores".[23] It was suggested that water molecules adsorb to polar groups presented on cuticular membrane (e.g. hydroxylic or ester groups), thus creating these pores.[24] Since lipophilic compounds can diffuse the cuticle via interaction with lipophilic domains,[25] it is possible that lipidated particles entry may be facilitated by sorption to cuticular lipids. Taken together, although several foliar penetration pathways are known and excessive work is being done to gain insights regarding tissue and cellular uptake mechanism,[26] it is still poorly understood how nanomaterials penetrate and translocate within plants.

2.3. dsRNA stability and release

To facilitate efficient knockdown, the RNA payload needs to be protected from degradation until reaching the target site. We tested the ability of the lmPEI carrier to protect dsRNA from RNase-A (ribonuclease) degradation. More specifically, we assessed the protection capacity of the complex against RNase-A before and after releasing the dsRNA from the particles and demonstrated that complexation with lmPEI protected the RNA from degradation (Figure 3A). We used heparin to release the RNA from the complex. Heparin is a highly negatively-charged molecule that competes with dsRNA for electrostatic interactions, releasing the dsRNA from the lmPEI complex (Figure S9).[27] Protection from RNase degradation was similar for RdRp and CP sequences, suggesting that the particle protection against nuclease degradation is independent of the RNA sequence (Figure 3C). In cells, it is suggested that the 'proton sponge' effect is in charge of releasing the RNA from amine-based RNA carriers, such as lmPEI. In addition, the "proton sponge" effect was documented in mammalian cells to trigger the endosomal escape of nanoparticles and their payload to the cytoplasm.[28] Plant cells contain a trans-Golgi network and multivesicular body similar to early and late endosomes, respectively.[29] Endosomal pH, being the main parameter affecting cationic polymer buffering capacity, is similar in both mammalian (pH=6.3) and plant (pH=6.2) cells,[30] thus suggesting the "proton sponge" effect may exist in both cell types.[28b, 31]

2.4. Field experiments – antiviral activity of lmPEI-dsRNA particles

To test the antiviral activity of the dsRNA-lmPEI particles, the ability to knockdown GLRaV-3 in infected vines was evaluated. For this, three field experiments were conducted in vineyards located in the Judean foothills in central Israel during the summer months (June-September) of years 2018, 2019 and 2020. Experiments took place in a Cabernet Sauvignon plot (31°50'17"N, 34°53'57"E, 140 meters

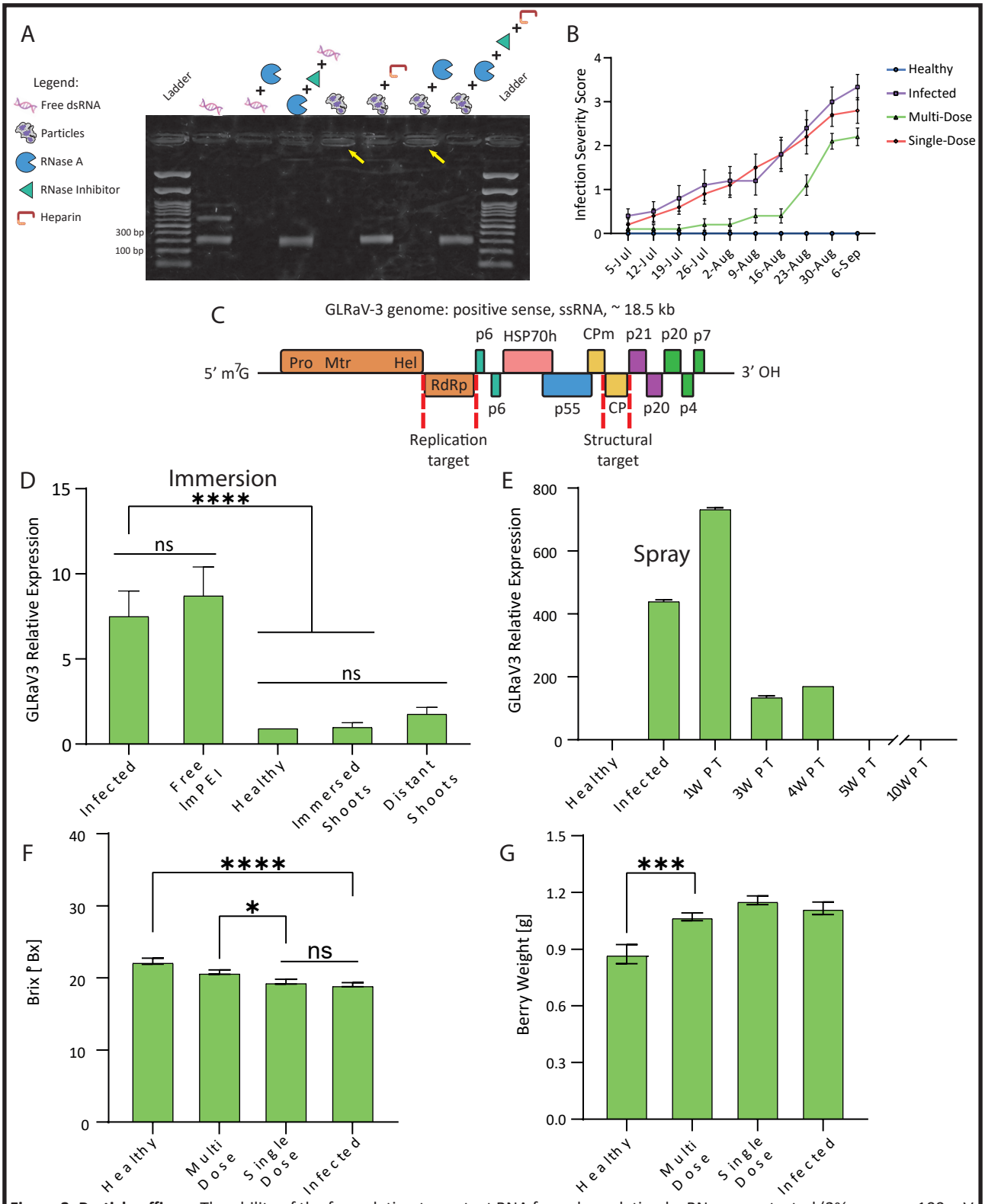

Figure 3: Particle efficacy The ability of the formulation to protect RNA from degradation by RNase was tested (2% agarose, 100 mV, 35 minutes, A). Naked RNA is degraded by RNase A (third well to the left) as opposed to maintaining RNA integrity when complexed with lmPEI in particle form (yellow arrows). Moreover, dsRNA integrity is kept identical when released from complexes or when released from complexes after RNase A treatment (second and fourth well to the right), proving complexes' ability to protect dsRNA from degradation. Infection severity scoring carried out throughout the 2020 field experiment shows delayed GLD symptoms in multi-dose treated vines in comparison to single dose (B). An illustration of grapevine leafroll associated virus 3 open reading frames with replication and structural RNAi targets (red dashed lines; C). Compared to untreated infected vines, GLRaV3 expression is downregulated after a single administration of RNA particles in the 2018 field experiment. Knockdown is recorded within the shoot tissue distant from immersion treatment point (D). Respectively, change in administration method to canopy spraying managed to retain virus down-regulation three weeks post treatment (PT) (E). Grape quality parameters of Brix (F) and berry weight (G) acquired after 2020 harvest indicating multiple treatments are preferable over a single treatment in recovering berries and suggests that multiple administrations may be needed to fully recover fruit quality. Results are shown as mean ± SD. Ordinary one-way ANOVA tests were used for statistical analysis of D, F and G. ns – not significant, *p<0.05, ***p<0.001, ****p<0.0001.

above sea level) grafted upon Ruggeri rootstock planted in soil mainly composed of clay, sand, and silt.[32] Vines were randomly divided into treatment groups by creating spaced blocks which were evenly spread across each row. To follow GLD symptoms throughout the experiments, an infection severity assessment table (Table S3) was designed, and half of each treatment group was scored once a week. At the end of each experiment, the shoots were pruned, and RT-PCR analysis was performed to assess GLRaV-3 titer within phloem tissue. Additionally, upon harvest, the berries were tested for grape quality parameters. Two different administration methods were applied as a single dose in 2018 and 2019 while multi-dose treatment was examined in 2020. In 2018 (N=28), to allow infiltrate uptake, leaves were brushed with particle solution and shoots were cut and immersed into treatment infiltrate for 24 hours (Figure S10A). In 2019, vines (N=47) were treated mainly by canopy spraying (Figure S10B) and only a few by shoot immersion to serve as a control. In 2020, vines (N=80) were treated only by canopy spraying either with a single or multi-dose (five treatments). In all consecutive years, there was a significant difference in GLRaV-3 titer between healthy and infected groups as well as between infected and particle-treated groups ($P<0.0001$; Figure 3D, S11 and S12). These results imply that the dsRNA-lmPEI particles penetrated and distributed within the vine, inducing viral knockdown.[26e, 33] Moreover, gene knockdown RT-PCR levels show that three weeks after a single-dose administration the virus titer decreased (Figure 3E). In contrast to virus expression, GLD symptoms improved only when the vine was treated multiple times throughout the growing season (Figure 3B). The berries' Brix and weight values were measured after harvest. Brix values indicate a single dose was not sufficient to cause recovery in infected berries, whereas a multi-dose treatment significantly improved sugar level within the infected fruits bringing it nearer to healthy berries' values ($P<0.05$, Figure 3F). This effect was measured to a lower extent in berry weight, suggesting

repeated treatment is superior in improving the viral symptoms. Additional parameters such as pH, total acid, tannin index, color density and softness ratio were examined at different time points after veraison (Figure S13-S17). As ripening progressed, pH levels increased, acidity levels decreased and there was an overall tendency for tannin index to elevate, demonstrating that dsRNA-lmPEI administration did not harm grape quality parameters of the treated vines. Therefore, this suggests that a single dose application of dsRNA-lmPEI is sufficient to reduce the viral titer, but multiple applications are needed to achieve full recovery of fruit quality.

3. Conclusion

GLD infects agricultural vineyards around the world damaging crop quality without efficient treatment options.[6] Our findings show that dsRNA-lmPEI particles carry, protect and release dsRNA efficiently, thereby constituting an effective delivery system for long agricultural dsRNA. RNAi particles distribute and accumulate within the grapevine's transportation system enabling a systemic effect throughout the vine. Lipidated particles increase the uptake rate into plant tissue compared to non-lipidated particles, offering molecular approaches for improving RNA delivery to crops. Stomate opening dimensions on the leaf surface, an order of magnitude larger than the particles facilitate a possible internalization route for particles into crops. Applied in two distinct administration methods, a single dose of particles downregulated GLRaV-3 titer and led to systemic reduction of the virus titer. Conversely, to achieve fruit quality recovery multiple treatment cycles are needed during the 4-6 months long growing season. Looking forward, the implementation of nanoparticle delivery systems in agriculture holds great promise. Yet, for wide scale agricultural application, studying the residence-time of these particles in crops, and ensuring minimal environment toll through water runoff or air

drift are important steps prior to large-scale agricultural implementation.[34] Overall, this study demonstrates that dsRNA-lmPEI particles act as a biological, non-GMO contender to treat GLRaV-3 infections in vines via foliar application. These findings may also be leveraged to treat other viral infections in food crops.

4. Experimental Section

4.1. Modified branched Polyethylenimine synthesis

Branched Polyethylenimine (Mw=800 gr/mol, Sigma-Aldrich - Merck) was conjugated with 1,2-Epoxytetradecane (Tokyo chemical industry co.) to formulate 14 carbon lipid-conjugated branched PEI. Conjugation was conducted through an epoxide ring opening reaction, maintaining a 3:1 molar ratio (Epoxide:bPEI) mixture. Briefly, 4.75 gr of bPEI were dissolved into 150 mL of pure ethanol and heated (55°C) to reach homogenous solution. Next, pre-calculated epoxide volume was added to the solution while keeping vigorous mixing. Mixture was incubated for 4 hours maintaining constant heating (90°C) and mixing (600 rpm) using thermocouple. After reaction was completed, verification of successful reaction was performed by loading 2 µl of 20-fold diluted reaction product in ethanol on a silica-coated thin-layer chromatography plate (Biotage) with Chloroform:n-Hexane 1:1 v/v as the mobile phase.

4.2. lmPEI purification and ^{1}HNMR analysis

Following the described synthesis, ethanolic phase in the product mixture was evaporated using B-300 rotary evaporator (Buchi, Switzerland) for several minutes at 40° C. Next, pure n-Heptane was

added to suspend unconjugated epoxide and sample was centrifuged at 17,000 xg for five minutes in RT. Suspension was removed from precipitate and sedimentation step was repeated twice to reach complete separation. Purified product was dried, resuspended in pure ethanol and 20 mg were taken for 1HNMR analysis. Neat reactants and purified lmPEI spectra were achieved using Bruker AVIII (Avance III)-400MHz and data was analyzed with ACD/Labs version 11.03 software. Pure PEI spectra shows multiple peaks at 2.48-2.65 ppm corresponding to non-labile hydrogen atoms where pure epoxide spectra display main peaks at 0.88, 1.26 and 2.45-2.93 ppm corresponding to aliphatic CH_3, CH_2 and hydrogen atoms comprising the cyclic three-atom ring. Product spectra reveals new peak at 3.62 ppm corresponding to CH-O- functional group.

4.3. dsRNA-lmPEI complexation based on N:P determination

Complexation based on electrostatic interaction between dsRNA and lmPEI was conducted by applying ethanol injection technique. N:P ratio is defined as the ratio between positively charged amine groups and negatively charged phosphate groups and plays an important role in complexation calculations. To achieve a desired N:P ratio, a constant amount of dsRNA was converted to its equivalent phosphate mole considering its length and double strand structure. Next, amine moles were calculated according to a desired N:P ratio and lmPEI dilution factor was derived from physical properties such as molecular weight and number of amine groups in a repeating unit. For example, 36 mg of dsRNA are equal to approximately 0.0001 mole of negatively charged phosphate groups. To reach N:P ratio of 2:1, we need approximately 0.0002 mole of amine groups. Given lmPEI branched amine structure and expected molecular weight after epoxide conjugation (1437.11 gr/mol), amine moles can be converted into lmPEI weight (0.046 gr). Based on a known volume used in ethanol

injection (50 mL), a weight concentration can be extracted (0.00092 gr/mL) and translated into a dilution factor (x32 dilution) needed to reach the desired lmPEI weight concentration adequate for N:P ratio of 2:1. In general, pre-heated dsRNA and lmPEI were added to 25 mM sodium acetate buffer (pH=5.2) in 1:1 v/v ratio, keeping a 2:1 N:P molar ratio. lmPEI was injected using a pipettor while vigorous mixing was achieved by vortex. Subsequently, mixture was incubated in Eppendorf shaker for 20 minutes at 40°C and 1000 rpm. Total particles concentration measured 5.091E+07 particles/mL and further characteristics such as size distribution, stability and mean diameter and charge were determined at room temperature by multi-angel (173˚, 13°) dynamic light scattering using Zetasizer Pro (Malvern, United Kingdom).

4.4. dsRNA retention and release

Evaluation of dsRNA complexation and its release was assessed using Heparin release assay. Heparin is a strong negatively charged molecule that can compete with dsRNA for electrostatic interactions, thus releasing it from particles. Following particles formation, 1 µl of diluted Heparin sodium salt (0.14 $_M$) from porcine intestinal mucosa (Sigma-Aldrich) was added to approximately 250 ng of complexed dsRNA and incubated for 20 minutes at 35°C. Subsequently, 2% gel agarose (Hy-Labs) in TAE (X1) with Ethidium Bromide (Hy-labs) was visualized under UV light after 35-minute run at 100 V.

4.5. RNase assay

Particle's ability to protect dsRNA from degradation was examined using RNase A (Thermo-Scientific, Cat. EN0531) and RiboLock RNase Inhibitor (Thermo-Scientific, Cat. EO0381). Briefly, 20 µl of dsRNA-lmPEI particles (approximately 700 ng dsRNA) were incubated with 2 ng RNase A for 2 hours at 37°C

following enzyme inactivation through incubation with RiboLock RNase Inhibitor (20 units per 70 ng of complexed dsRNA) for 1 hour at 37°C. Next, solution was incubated with diluted Heparin for another 20 minutes at 37°C to release dsRNA from particles. Final product was applied with adequate controls to a 2% agarose gel electrophoresis for 35 minutes at 100 V.

4.6. cryo-TEM imaging and Fast Fourier Transformation analysis

Cryogenic transmission electron microscopy (cryo-TEM) imaging was performed by Technion Center for Electron Microscopy of Soft Matter (TCEMSM) on a Thermo-Fisher Talos F200C, FEG-equipped high resolution-TEM, operated at 200kV. Specimens were transferred into a Gatan 626.6 cryo-holder and equilibrated below -170 °C. Micrographs were recorded by a Thermo-Fisher Falcon III direct detector camera, at a 4k x 4k resolution. Specimens were examined at TEM nanoprobe mode using volta phase plates for contrast enhancement. Imaging was performed at a low dose mode of work to minimize the exposure of the imaged area to electrons. Images were acquired using the TEM Imaging and Acquisition (TIA) software. Inter-fiber spacing was deduced by performing radial integration on FFT of the relevant obtained images. Integration was done using FIJI software plugin by Paul Baggethun, 2009 version.

4.7. Cy5-lmPEI labeling

To visualize particles under microscopy instrumentation, amine-reactive red emitting fluorescent dye Cyanine5 NHS ester (Ex/Em:646/662nm, Abcam) was conjugated to lmPEI prior dsRNA complexation through carbodiimide reaction using NHS as a coupling reagent. Following epoxide ring opening reaction described previously Cy5 NHS ester and lmPEI were reacted in 1:4 ($Cy5:NH_2$) molar ratio and

incubated for 90 minutes at 37°C, 600 rpm to yield Cy5-lmPEI. One step size exclusion procedure was held using G-10 Sephadex beads (Sigma Aldrich) to isolate desired product from raw reactants and other by products. Each step of the process was verified using TLC with Chloroform:Methanol 1:1 v/v as the mobile phase.

4.8. Fluorescent Microscopy

To investigate particles uptake by vine leaves following spray and immersion administration routes, Cy5-labeled dsRNA-lmPEI were synthesized and complexed as described above. In addition, free Cy5 was treated the same as labeled particles to be administered as control. Vine leaves were divided into five treatment groups (N=5 per group) as follows: 25mM sodium acetate buffer (pH-5.2), sprayed particles, spray control, immersion particles and immersion control. Immersion leaves' petioles were embedded into 600 µl of infiltrate treatment whereas sprayed leaves were sprayed with treatment to reach seepage (~10 mL). Each group was imaged after 2 hours and six different locations were chosen within each leaf to best average total image signal. Samples were exposed for 400 ms and images were obtained using Olympus SZX16 fluorescent binocular equipped with DP72 CCD camera combined with x1.6 (NA 0.3) objective lens and Olympus mcherry filter (Excitation: 542-582, Emission: 603-678). Arabidopsis roots were divided into five treatment groups (N=4 per group) as well: Cy5-labeled lipidated and non-lipidated particles, non-labeled lipidated and non-lipidated particles and free Cy5. Each group was placed on an optical plate as described previously[35] and treated with 20 µl solution. Fluorescent signals were detected at initial time and after 3 hours using a LSM 710 inverted confocal laser-scanning microscope (Zeiss) with a x40 water objective lens (NA 1.2). eGFP (greens) and Cy5-lmPEI-dsRNA particles (reds) were viewed at excitation wavelengths of 488 nm and 639 nm

lasers, respectively. Fluorescence emission was detected at 675 nm for reds and with a 500-530 nm bandpass filter for greens.

4.9. Plant material, growth conditions and chemical treatments

All Arabidopsis (*Arabidopsis thaliana*) lines were in the Columbia-0 (Col-0) background. The following lines were used: p35S-eGFP-Lti6b[36], pUBQ10-PM-tdTomato[37] and wild-type. Seeds were sterilized and germinated on one-half-strength Murashige and Skoog (MS) medium supplemented with 0.2% (w/v) sucrose. Plates with sterilized seeds were stratified in the dark for 2 days, at 4°C, and then transferred to 22°C and to a 16h light/8h dark cycle (70 µmol m^{-2} s^{-1}), for 7 days.

4.10. Gd-labeled particles and biodistribution study

To prove and track particle distribution within vines, a rare earth metal Gadolinium was covalently conjugated to RNA carrier. After carrier synthesis, DOTA-NHS (0.036 gr, CheMatech, France) was added to lmPEI to reach 1:9 (lmPEI:DOTA-NHS) molar ratio followed by a four-hour incubation in alkaline environment. Next, DOTA-lmPEI was dried using rotary evaporator (130 rpm, 40°C, 2 mbar) and resuspended in pure ethanol to test for successful reaction using TLC. A 10-fold excess of Gadolinium(III) chloride hexahydrate (0.032 gr, Merck, Israel) was added to ensure all DOTA sites capture Gadolinium and another four-hour incubation was held in alkaline environment. To remove unwanted substances, Gd-DOTA-lmPEI was first complexed with dsRNA to generate particles that were later dialyzed over-night using a 12–14kDa dialysis membrane (Spectrum Labs, Breda, Netherlands) against complexation buffer (25 mM sodium acetate, pH 5.2). One leaf from medium sized vine seedlings (N=3) was embedded within Gd-labeled particle solution for 72-hour period. For

negative control, the same setup included the submersion into a non-labeled particle solution. Different tissues such as leaves, petioles, stem and roots were taken above and below submersion point. Tissues were dehydrated in a laboratory furnace (BIFA Electro-therm MS8, Middlesex, UK) for 2 hours at 120°C. Dry matter was weighted and cremated for 5 hours at 550°C. Ash samples were dissolved in 10 mL 1% HNO_3, filtered (0.45 μm filter) and analyzed for Gadolinium presence by ICP-OES apparatus (Agilent). Quantification was enabled using pre-prepared calibration curve obtained with Gd ICP standard (Sigma Aldrich).

4.11. HR-SEM imaging

High resolution scanning electron microscopy (HR-SEM) imaging was performed by Technion Center for Electron Microscopy of Soft Matter (TCEMSM) on a Zeiss Ultra Plus high-resolution SEM, equipped with a Schottky field-emission gun. Specimens were imaged at low acceleration voltages of 1.1 kV and a working distance of 3.6 mm. We used the Everhart Thornley ("SE2") secondary electron imaging detector.

4.12. Field experiments

Field trials (2018, 2019 and 2020) were conducted at 'Bravdo' vineyard located near Carmi Yossef, Israel. Vines showed various symptoms consistent with GLRaV3 infection, from small red dots on leaves to leaves that are completely red and curled inwards. At first experiment (June-September 2018), total of 28 vines were selected and divided into seven treatment groups (N=4) as follows: 1) Untreated healthy vines; 2) Untreated infected vines; 3) Infected vines treated with 25mM Sodium acetate buffer; 4) Infected vines treated with lmPEI solution; 5) Infected vines treated with naked

RdRp sequence; 6) Infected vines treated with RdRp-lmPEI particles; 7) Infected vines treated with both RdRp-lmPEI and CP-lmPEI particles. To improve infiltrate's uptake, two administration methods were employed - selected leaves were brushed with 5 mL of treatment solution and trimmed shoots were embedded within 20 mL of treatment solution for 24-hour period. Shoots and berries were taken for further analysis 6, 10 and 21 days and 8- and 9-weeks post treatment, respectively. At following year (June-September 2019), administration methods used were canopy spraying and shoot immersion. Total of 47 vines were distributed to construct the following treatment groups (N=10, except group number 4 where N=7): 1) Untreated healthy vines; 2) Untreated infected vines; 3) Healthy vines sprayed with lmPEI solution; 4) Infected vines' trimmed shoots immersed within both RdRp-lmPEI and CP-lmPEI particles; 5) Infected vines sprayed with both RdRp-lmPEI and CP-lmPEI particles. Shoots were sampled at harvest whereas berry collection took place 3,5 and 8 weeks after veraison. In the 2020 field experiment (June-September), a manual back-sprayer was used to spray each vine with 400 mL of the RdRp-lmPEI and CP-lmPEI particle solution to reach seepage. Spraying took place every two weeks half an hour before sunrise. Total of 80 vines were divided into four treatment groups (N=20 per group): 1) Untreated healthy vines; 2) Untreated infected vines; 3) Single dose treated infected vines; 4) Multi-dose treated infected vines (sprayed five times). Shoots were sampled before applying the first treatment, at the middle of the experiment and at harvest. Berry collection took place at harvest and once a week after veraison from ten constant vines in each treatment for an on-site Brix measurement. Six berries were samples from three different locations on the same cluster. In addition, to follow GLD symptoms throughout the experiment and further evaluate GLRaV-3 effect on leaves phenotype, ten constant vines from each treatment group were

visually tested and scored in a scale of 0-4 according to their severity symptoms by a pre-determined table (Table S3).

4.13. RNA extraction and cDNA production

Random shoots were pruned, leaves were disposed, and periderm was peeled off using a scalpel exposing inner tissues. Next, xylem was peeled out retaining the green phloem immediately frozen in liquid nitrogen and eventually transferred to – 80°C. 500 mg of frozen phloem was ground to a powder in liquid nitrogen using mortar and pestle. Total RNA was extracted using a Cetyltrimethyl Ammonium Bromide (CTAB)-based extraction protocol.[38] Another approach used for RNA extraction was using industrial Spectrum™ Plant Total RNA Kit (Sigma-Aldrich) following the manufactures' instructions. After RNA was extracted from the shoots, RNA purity and quantity were evaluated using Nanodrop spectrophotometer; RNA integrity was assessed using gel-electrophoresis. Lastly, total cDNA was collected using Maxima First Strand (Thermo Fisher Ltd) and qScript® (QuantaBio) cDNA Synthesis Kit for RT-qPCR following the manufacturer's protocol.

4.14. GLRaV identification

cDNA was amplified using specific primers (Table S1) for various GLRaV strains by polymerase chain reaction (PCR). 2X PCRBIO Taq Mix Red (PCRBIOSYSTEMS) PCR kit was used. PCR products were sent to HyLabs IL Ltd for Sanger sequencing, without further purification.

4.15. Viral titer assessment

Quantitative real-time PCR (qRT-PCR) was performed using Power SYBR™ Green PCR Master Mix (Thermo Fisher Ltd, Applied Biosystems™) and qPCR BIO SyGreen Mix (PCRBIOSYSTEMS) with cycling conditions implemented according to manufacturer's instructions in Rotor-Gene™ 6000 (Corbett Research Ltd), qTOWER3 (Analytik Jena AG) and QuantStudio1 (Applied Biosystems^{TM}) real-time PCR thermal cyclers. Before operating qRT-PCR, specific primers were evaluated for their amplification efficiencies (Table S2) as well as confirmed with standard controls of non-template control minus reverse transcriptase control. Moreover, primers specificity was tested any analyzing dissociation curve ranging from 60°C to 95°C. GLRaV-3 Relative expression was calculated based on $2^{-\Delta\Delta Ct}$ method.[39]

4.16. Grape quality parameters

Berries were tested for Brix (sugar) levels, weight, pH levels, color density, tannin index and softness ratio. Each vine's berries were crushed, and the mixture was filtered using a strainer to measure brix. For acidity measurement, 10 mL of the same mixture were taken and tittered using 0.1N NaOH until pH reached 8.15. The volume of NaOH needed was used to calculated total acid content as follows: 0.75*NaOH volume. Tartaric acid correction was done to mimic wine's natural acidity level. To calculate averaged berry weight, fresh batch of berries were weighed, counting the number of berries needed to reach 132 grams. Pure ethanol was added to constitute 12% by weight/volume and the berries were crushed. After 48 hours precipitation in 4°C mixture was centrifuged at 1500 rpm for 10 minutes. To assess optical density (OD), mixture was diluted 25-fold and OD was measured using a spectrophotometer at wavelength of 520 and 420 nm. Furthermore, color density was calculated as follow: (25∗OD420nm) + (25∗OD520nm). To evaluate the tannin index (total phenols), mixture was

diluted 100-fold, then measured using spectrophotometer at wavelength of 280 nm. Tannin index was calculated as follows: (100∗OD280nm). Lastly, softness ratio was calculated as 10*(color density/tannin index).

During harvest of summer 2019 and 2020, the total yield of the grapes harvested from each vine was calculated.

4.17. Statistical analysis and image acquisition

Data is presented as mean values and error bars indicate SD. Statistical studies such as ordinary two-way ANOVA in Figure 2 and multiple comparison of one-way ANOVA in Figure 3 were conducted using Prism software version 9.0. Gel, binocular, and confocal images were processed using ZEN and Fiji software. HR-SEM image was processed using Adobe Photoshop 2021. Particles were identified using Imaris 9.1.2 software (Oxford, Bitplane) spots module to detect spots as spherical objects with 0.2 µm diameter and quality threshold value above 3.

Supporting Information

Supporting Information is available from the Wiley Online Library or from the author.

Acknowledgements

This project has received funding from the European Union's Horizon 2020 research and innovation program under grant agreement No 680242-ERC-[Next-Generation Personalized Diagnostic Nanotechnologies for Predicting Response to Cancer Medicine].

The authors also acknowledge the support of the Technion Integrated Cancer Center (TICC), the Russell Berrie Nanotechnology Institute, the Lorry I. Lokey Interdisciplinary Center for Life Sciences & Engineering, The Israel Ministry of Economy for a Kamin Grant (52752, 69230); the Israel Ministry of Science Technology and Space – Office of the Chief Scientist (3-11878); Israel Innovation Authority for Nofar Grant (67967), the Israel Science Foundation (1778/13, 1421/17); the Israel Ministry of Science & Technology (3-16963) ; Ministry of Agriculture & Rural Development - Office of the Chief Scientist (323/19); the Israel Ministry of Science and Technology (3-17418); the Israel Cancer Association (2015-0116); Leventhal 2020 COVID19 Research Fund (ATS #11947), the German-Israeli Foundation for Scientific Research and Development for a GIF Young grant (I-2328-1139.10/2012); the European Union FP-7 IRG Program for a Career Integration Grant (908049); the Phospholipid Research Center Grant (ASC-2018-062/1-1); the Louis family Cancer Research Fund, a Mallat Family Foundation Grant; The Unger Family Fund; a Carrie Rosenblatt Cancer Research Fund, A. Schroeder acknowledges Alon and Taub Fellowships. The authors also acknowledge Dr. Nitsan Dahan for his help during the microscopy analysis. The help of Dr. Ruth Jalfon in editing this manuscript is greatly appreciated. Images in this paper were created with Adobe Illustrator and BioRender.com.

References

[1] L. F. Bisson, A. L. Waterhouse, S. E. Ebeler, M. A. Walker, J. T. Lapsley, *Nature* **2002**, 418, 696.

[2] a) O. J. Alabi, L. F. Casassa, L. R. Gutha, R. C. Larsen, T. Henick-Kling, J. F. Harbertson, R. A. Naidu, *PLoS One* **2016**, 11, e0149666; b) S. S. Atallah, M. I. Gomez, M. F. Fuchs, T. E. Martinson, *American Journal of Enology and Viticulture* **2011**, 63, 73.

[3] R. A. Naidu, H. J. Maree, J. T. Burger, *Annu Rev Phytopathol* **2015**, 53, 613.

[4] R. Montero, D. Mundy, A. Albright, C. Grose, M. C. Trought, D. Cohen, K. M. Chooi, R. MacDiarmid, J. Flexas, J. Bota, *Food Chem* **2016**, 197 Pt B, 1177.

[5] S. T. Endeshaw, P. Sabbatini, G. Romanazzi, A. C. Schilder, D. Neri, *Scientia Horticulturae* **2014**, 170, 228.

[6] H. J. Maree, R. P. Almeida, R. Bester, K. M. Chooi, D. Cohen, V. V. Dolja, M. F. Fuchs, D. A. Golino, A. E. Jooste, G. P. Martelli, R. A. Naidu, A. Rowhani, P. Saldarelli, J. T. Burger, *Front Microbiol* **2013**, 4, 82.

[7] G. P. Martelli, Agranovsky, A.A., Bar-Joseph, M., Boscia, D., Candresse, T., Coutts, R.H.A., Dolja, V.V., Hu, J.S., Jelkmann, W., Karasev, A.V., Martin, R.R., Minafra, A., Namba, S. and Vetten, H.J, *Virus Taxonomy*, **2012**.

[8] a) R. Almeida, K. Daane, V. Bell, G. K. Blaisdell, M. Cooper, E. Herrbach, G. Pietersen, *Frontiers in Microbiology* **2013**, 4; b) R. Naidu, A. Rowhani, M. Fuchs, D. Golino, G. P. Martelli, *Plant Dis* **2014**, 98, 1172; c) V. I. Maliogka, G. P. Martelli, M. Fuchs, N. I. Katis, *Adv Virus Res* **2015**, 91, 175.

[9] A. Fire, S. Xu, M. K. Montgomery, S. A. Kostas, S. E. Driver, C. C. Mello, *Nature* **1998**, 391, 806.

[10] D. Baulcombe, *Nature* **2004**, 431, 356.

[11] a) T. Holen, M. Amarzguioui, E. Babaie, H. Prydz, *Nucleic Acids Research* **2003**, 31, 2401; b) J. Martinez, A. Patkaniowska, H. Urlaub, R. Lührmann, T. Tuschl, *Cell* **2002**, 110, 563; c) H. J. Haringsma, J. J. Li, F. Soriano, D. M. Kenski, W. M. Flanagan, A. T. Willingham, *Nucleic Acids Research* **2012**, 40, 4125.

[12] G. Meister, T. Tuschl, *Nature* **2004**, 431, 343.

[13] a) C. A. Brosnan, O. Voinnet, *Current Opinion in Plant Biology* **2011**, 14, 580; b) P. Dunoyer, G. Schott, C. Himber, D. Meyer, A. Takeda, J. C. Carrington, O. Voinnet, *Science* **2010**, 328, 912; c) C.-G. Duan, C.-H. Wang, H.-S. Guo, *Silence* **2012**, 3, 5; d) K. E. Robinson, E. A. Worrall, N. Mitter, *Journal of Plant Biochemistry and Biotechnology* **2014**, 23, 231.

[14] S. Ufaz, A. Balter, C. Tzror, S. Einbender, O. Koshet, J. Shainsky-Roitman, Z. Yaari, A. Schroeder, *Molecular Systems Design & Engineering* **2018**, 3, 38.

[15] a) A. T. Silva, A. Nguyen, C. Ye, J. Verchot, J. H. Moon, *BMC Plant Biology* **2010**, 10, 291; b) T. M. Burch-Smith, J. C. Anderson, G. B. Martin, S. P. Dinesh-Kumar, *Plant J* **2004**, 39, 734; c) D. Gan, J. Zhang, H. Jiang, T. Jiang, S. Zhu, B. Cheng, *Plant Cell Reports* **2010**, 29, 1261.

[16] a) A. G. Reynolds, in *Managing Wine Quality*, DOI: https://doi.org/10.1533/9781845699284.3.365 (Ed: A. G. Reynolds), Woodhead Publishing **2010**, p. 365; b) I. Pertot, T. Caffi, V. Rossi, L. Mugnai, C. Hoffmann, M. S. Grando, C. Gary, D. Lafond, C. Duso, D. Thiery, V. Mazzoni, G. Anfora, *Crop Protection* **2017**, 97, 70; c) D. R. Walters, J. Ratsep, N. D. Havis, *Journal of Experimental Botany* **2013**, 64, 1263; d) M. Wenneker, M. M. Riemens, B. Allema, J. Bremmer, D. Van Apeldoorn, Y. Bai, C. Kempenaar, M. Reinders, *Future of crop protection in Europe*, **2021**.

[17] A. L. Jackson, J. Burchard, J. Schelter, B. N. Chau, M. Cleary, L. Lim, P. S. Linsley, *RNA* **2006**, 12, 1179.

[18] a) K. A. Whitehead, R. Langer, D. G. Anderson, *Nat Rev Drug Discov* **2009**, 8, 129; b) P. Kesharwani, V. Gajbhiye, N. K. Jain, *Biomaterials* **2012**, 33, 7138.

[19] a) A. K. Mishra, H. Weissman, E. Krieg, K. A. Votaw, M. McCullagh, B. Rybtchinski, F. D. Lewis, *Chemistry – A European Journal* **2017**, 23, 10328; b) P. P. Neelakandan, Z. Pan, M. Hariharan, Y. Zheng, H. Weissman, B. Rybtchinski, F. D. Lewis, *Journal of the American Chemical Society* **2010**, 132, 15808.

[20] C. Sun, T. Tang, H. Uludağ, Javier E. Cuervo, *Biophysical Journal* **2011**, 100, 2754.

[21] J. Ziebarth, Y. Wang, *Biophysical Journal* **2009**, 97, 1971.

[22] A. Berhin, D. de Bellis, R. B. Franke, R. A. Buono, M. K. Nowack, C. Nawrath, *Cell* **2019**, 176, 1367.

[23] a) L. Schreiber, *Ann Bot* **2005**, 95, 1069; b) V. Fernández, T. Eichert, *Critical Reviews in Plant Sciences* **2009**, 28, 36; c) T. Eichert, H. E. Goldbach, *Physiologia Plantarum* **2008**, 132, 491.

[24] P. LUQUE, R. GAVARA, A. HEREDIA, *New Phytologist* **1995**, 129, 283.

[25] a) L. Schreiber, *J Exp Bot* **2006**, 57, 2515; b) A. Buchholz, *J Exp Bot* **2006**, 57, 2501.

[26] a) G. Chichiriccò, A. Poma, *Nanomaterials (Basel)* **2015**, 5, 851; b) P. Miralles, T. L. Church, A. T. Harris, *Environmental Science & Technology* **2012**, 46, 9224; c) L. Zhao, J. R. Peralta-Videa, A. Varela-Ramirez, H. Castillo-Michel, C. Li, J. Zhang, R. J. Aguilera, A. A. Keller, J. L. Gardea-Torresdey, *Journal of Hazardous Materials* **2012**, 225-226, 131; d) E. Onelli, C. Prescianotto-Baschong, M. Caccianiga, A. Moscatelli, *Journal of Experimental Botany* **2008**, 59, 3051; e) C. Palocci, A. Valletta, L. Chronopoulou, L. Donati, M. Bramosanti, E. Brasili, B. Baldan, G. Pasqua, *Plant Cell Reports* **2017**, 36, 1917.

[27] M. Bertschinger, G. Backliwal, A. Schertenleib, M. Jordan, D. L. Hacker, F. M. Wurm, *Journal of Controlled Release* **2006**, 116, 96.

[28] a) R. V. Benjaminsen, M. A. Mattebjerg, J. R. Henriksen, S. M. Moghimi, T. L. Andresen, *Mol Ther* **2013**, 21, 149; b) N. D. Sonawane, F. C. Szoka, Jr., A. S. Verkman, *J Biol Chem* **2003**, 278, 44826.
[29] A. L. Contento, D. C. Bassham, *Journal of Cell Science* **2012**, 125, 3511.
[30] J. Shen, Y. Zeng, X. Zhuang, L. Sun, X. Yao, P. Pimpl, L. Jiang, *Molecular Plant* **2013**, 6, 1419.
[31] a) M.-S. Roell, *Plant Physiology* **2020**, 184, 548; b) A. Akinc, M. Thomas, A. M. Klibanov, R. Langer, *J Gene Med* **2005**, 7, 657; c) J.-P. Behr, *CHIMIA International Journal for Chemistry* **1997**, 51, 34; d) R. K. Dhandapani, D. Gurusamy, J. L. Howell, S. R. Palli, *Scientific Reports* **2019**, 9, 8775.
[32] S. L. MacDonald, M. Staid, M. Staid, M. L. Cooper, *Computers and Electronics in Agriculture* **2016**, 130, 109.
[33] a) P. Teszlák, M. Kocsis, A. Scarpellini, G. Jakab, L. Kőrösi, *Photosynthetica* **2018**, 56, 1378; b) A. Valletta, L. Chronopoulou, C. Palocci, B. Baldan, L. Donati, G. Pasqua, *Journal of Nanoparticle Research* **2014**, 16, 2744.
[34] a) C. N. T. Taning, B. Mezzetti, G. Kleter, G. Smagghe, E. Baraldi, *Trends in Biotechnology* **2021**, 39, 644; b) P. Wang, E. Lombi, F.-J. Zhao, P. M. Kopittke, *Trends in Plant Science* **2016**, 21, 699; c) M. P. Landry, N. Mitter, *Nature Nanotechnology* **2019**, 14, 512; d) Y. Shang, M. K. Hasan, G. J. Ahammed, M. Li, H. Yin, J. Zhou, *Molecules* **2019**, 24, 2558.
[35] Y. Fridman, S. Strauss, G. Horev, M. Ackerman-Lavert, A. R. Benaim, B. Lane, R. S. Smith, S. Savaldi-Goldstein, *bioRxiv* **2021**, DOI: 10.1101/2021.04.01.4380112021.04.01.438011.
[36] S. R. Cutler, D. W. Ehrhardt, J. S. Griffitts, C. R. Somerville, *Proceedings of the National Academy of Sciences* **2000**, 97, 3718.
[37] Charles W. Melnyk, C. Schuster, O. Leyser, Elliot M. Meyerowitz, *Current Biology* **2015**, 25, 1306.
[38] B. Blanco-Ulate, E. Vincenti, A. Powell, D. Cantu, *Frontiers in Plant Science* **2013**, 4.
[39] K. J. Livak, T. D. Schmittgen, *Methods* **2001**, 25, 402.